Environment Canada

Environnement Canada

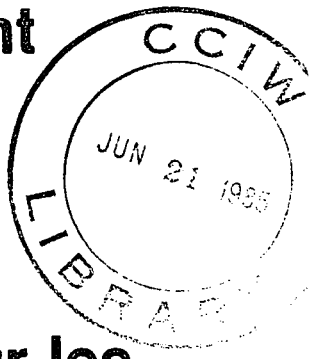

National Water Research Institute

Institut National de Recherche sur les Eaux

TURBULENCE MODELLING OF FLOOD PLAIN FLOWS

by

B.G. Krishnappan and Y.L. Lau

Krishnappan (47)

Lau (53)

This manuscript has been submitted to the
American Society of Civil Engineering for publication
and the contents are subject to change

This copy is to provide information prior to publication

TURBULENCE MODELLING OF FLOOD PLAIN FLOWS

by

B.G. Krishnappan and Y.L. Lau

Environmental Hydraulics Section
Hydraulics Division
National Water Research Institute
Canada Centre for Inland Waters

January 1985

ABSTRACT

A numerical model capable of predicting flow characteristics in a compound channel is described. The model solves the continuity and momentum equations along with the transport equations of kinetic energy of turbulence and the dissipation rate. Closure is achieved with the aid of algebraic relations for turbulence stresses. The model is capable of treating compound channels formed by regular geometrical sections of main channel and flood plain segments. The width of the main channel, the width of the total section, the depth of flow in flood plain, the total depth, channel slope and boundary roughness of main channel section and flood plain section can all be varied.

The model predictions of total flow rate, shear stress distributions around the wetted perimeter, and the percentage of flow and shear force carried by the different sections were compared with published experimental data. Reasonable agreement between data and predictions were obtained.

RÉSUMÉ

On présente un modèle capable de prévoir le régime d'écoulement des eaux dans un chenal multiple. Le modèle permet de résoudre les équations de continuité et de quantité de mouvement ainsi que les équations de transport de l'énergie cinétique de la turbulence et le taux de dispersion. La fermeture est réalisée au moyen de relations albégriques décrivant le cisaillement dû à la turbulence. Le modèle est capable d'analyser les chenaux multiples composés d'un chenal principal et de chenaux secondaires (à même le périmètre d'inondation) ayant une coupe régulière. On peut faire varier la largeur du chenal principal, la largeur de la coupe totale, la profondeur de l'écoulement dans le périmètre d'inondation, la profondeur totale, la pente du chenal et le degré d'irrégularité de la paroi du chenal principal et de la coupe du périmètre d'inondation.

On a comparé à des données expérimentales déjà publiées les prévisions du modèle relatives au débit total de l'écoulement, à la répartition de l'effort de cisaillement autour du périmètre mouillé et à la proportion de l'écoulement et de l'effort de cisaillement agissant sur les différentes coupes. Les données réelles et les prévisions concordent assez bien.

MANAGEMENT PERSPECTIVE

Once a river rises above its banks, the ultimate level, even if the flow is known, cannot be predicted with confidence. This paper examines the reliability of a model to predict levels and channel velocities where the boundary controlling roughnesses are known. The model has proved reliable. However, successive stages will look at the model performance in real flood plains.

Note that conversely the model would give more accurate estimates of maximum flood flows from the flood level.

T. Milne Dick
Chief
Hydraulics Division

PERSPECTIVE-GESTION

Lorsqu'un cours d'eau quitte son lit, on ne peut prévoir avec certitude le niveau maximal qu'atteindront les eaux même si l'on en connaît le débit. Le présent article porte sur la fiabilité d'un modèle ayant pour but de prévoir la vitesse d'écoulement et le niveau d'eau dans un chenal, si l'on connaît le degré d'irrégularité de ses parois. Le modele s'est revele fiable. A l'occasion d'essais ultérieurs, on examinera les résultats du modèle face à des périmètres d'inondation réels.

Il est à noter qu'inversement le modèle offre une estimation plus exacte du débit maximal des eaux en période de crues ou d'inondations à partir d'un niveau d'eau donné.

Le chef,
T. Milne Dick
Division de l'hydraulique

INTRODUCTION

Most natural streams have cross-sections which can be characterised as compound sections, i.e., a section consisting of a deep and narrow main channel overlain by wide and shallow flood plains. The river flow is contained within the main channel sections most of the time. However, during flood events the river spills over onto the flood plains, resulting in a compound-channel flow. Such flows are complicated by the momentum transfer between the flood plains and the main channel and are still not well understood. Most of the methods for calculating flows in compound channels rely on dividing the channel and flood plain into sections with imaginary boundaries and using some empirical relationships, derived from limited laboratory data, for the stress at the boundaries.

One and two-dimensional mathematical models have been used to compute flows with flood plains. However, the lateral momentum transfer and the secondary circulation in these compound channels mean that the flows are highly three-dimensional and that great difficulties would be encountered with the use of simple models. In this paper, a three-dimensional turbulence model has been applied to calculate flows in compound channels. Turbulence models have been used successfully to calculate the flow and the transfer of heat and mass in open channels (3, 8). Naot and Rodi (6) have also demonstrated the ability of a turbulence model to calculate secondary currents in open and closed channel flows. The present model has been used to calculate the flow and shear stress distributions in channels with compound cross-sections and the comparisons of model predictions with available laboratory data are presented in this paper.

MODEL DESCRIPTION

Governing Equations

The compound channel cross-section and the coordinate system are shown in Fig. 1. The grid system used in the model is such that the channel section can be either symmetrical as shown in Fig. 1 or asymmetrical, with the flood plain attached to only one side of the main channel. Both the main channel section and the flood plain section can be either square or rectangular.

The turbulence model used in this study is similar to the one proposed by Noat and Rodi (6). It is a version of the k-ε turbulence model which uses algebraic relationships for the turbulent stresses. However, the algebraic relationships and some of the surface conditions used are different from those in Ref. 6. The governing equations are listed below.

continuity equation:

$$\frac{\partial u}{\partial x} + \frac{\partial v}{\partial y} + \frac{\partial w}{\partial z} = 0 \quad \ldots\ldots\ldots\ldots\ldots\ldots \quad (1)$$

momentum equations:

in x direction

$$u \frac{\partial u}{\partial x} + v \frac{\partial u}{\partial y} + w \frac{\partial u}{\partial z} = -g \frac{\partial H}{\partial x} + g\sin\theta + \frac{\partial}{\partial y}\left((\nu + \nu_t) \frac{\partial u}{\partial y}\right)$$

$$+ \frac{\partial}{\partial z}\left((\nu + \nu_t) \frac{\partial u}{\partial z}\right) \quad \ldots\ldots \quad (2)$$

in y direction

$$u\frac{\partial v}{\partial x} + v\frac{\partial v}{\partial y} + w\frac{\partial v}{\partial z} = -\frac{\partial p}{\partial y} + \frac{\partial}{\partial y}\left(\nu\frac{\partial v}{\partial y}\right) + \frac{\partial}{\partial z}\left(\nu\frac{\partial v}{\partial z}\right)$$

$$-\frac{\partial}{\partial y}\overline{v'^2} - \frac{\partial}{\partial z}\overline{v'w'} \quad \ldots\ldots \quad (3)$$

in z direction

$$u\frac{\partial w}{\partial x} + v\frac{\partial w}{\partial y} + w\frac{\partial w}{\partial z} = -\frac{\partial p}{\partial z} + \frac{\partial}{\partial y}\left(\nu\frac{\partial w}{\partial y}\right) + \frac{\partial}{\partial z}\left(\nu\frac{\partial w}{\partial z}\right)$$

$$-\frac{\partial}{\partial y}\overline{w'v'} - \frac{\partial}{\partial z}\overline{w'^2} \quad \ldots\ldots \quad (4)$$

where u, v and w are time average velocities in the x, y and z directions respectively; u' v' and w' are the fluctuating components of u, v and w; p is the pressure and g is the acceleration due to gravity, H is the flow depth, θ is the inclination of the channel bottom to horizontal, ν is the kinematic viscosity of the fluid and ν_t is the eddy-viscosity. The turbulent shear stresses $\overline{v'^2}$, $\overline{w'^2}$ and $\overline{v'w'}$ are evaluated using the algebraic stress relations of Thatchell (10). Accordingly, these stresses are given by the following relations:

$$\overline{v'^2} = k\left(\frac{c_{\phi_1}}{c_{\phi_1}-2c_{\phi_2}}\right)\left[\frac{2}{3} - \frac{2-6\beta}{3c_{\phi_1}}\right] - 2\frac{\beta k}{\varepsilon}\left(\frac{\nu_t}{c_{\phi_1}-2_{\phi_2}}\right)\left(\frac{\partial u}{\partial y}\right)^2 \quad \ldots(5)$$

$$\overline{w'^2} = k\left(\frac{c_{\phi_1}}{c_{\phi_1}-2c_{\phi_2}}\right)\left[\frac{2}{3} - \frac{2-6\beta}{3c_{\phi_1}}\right] - \frac{2\beta k}{\varepsilon}\left(\frac{\nu_t}{c_{\phi_1}-2c_{\phi_2}}\right)\cdot\left(\frac{\partial u}{\partial z}\right) \quad \ldots(6)$$

and $$\overline{v'w'} = \frac{-2\beta}{c_{\phi_1}-2c_{\phi_2}} \frac{k}{\varepsilon} \nu_t \frac{\partial u}{\partial y} \frac{\partial u}{\partial z} \quad \ldots\ldots\ldots\ldots\ldots \quad (7)$$

In equations 5, 6 and 7, k is the turbulent kinetic energy, ε is the dissipation rate of turbulent energy, c_{ϕ_1}, c_{ϕ_2} and β are empirical constants. The kinetic energy k and dissipation rate ε are evaluated using the k-ε model developed at Imperial College (9) and the equations of k and ε are

$$u \frac{\partial k}{\partial x} + v \frac{\partial k}{\partial y} + w \frac{\partial k}{\partial z} = \frac{\partial}{\partial y} \left(\frac{\nu_t}{\sigma_k} \frac{\partial k}{\partial y}\right) + \frac{\partial}{\partial z} \left(\frac{\nu_t}{\sigma_k} \frac{\partial k}{\partial z}\right) + P-\varepsilon \quad (8)$$

$$u \frac{\partial \varepsilon}{\partial x} + v \frac{\partial \varepsilon}{\partial y} + w \frac{\partial \varepsilon}{\partial z} = \frac{\partial}{\partial y}\left(\frac{\nu_t}{\sigma_\varepsilon} \frac{\partial \varepsilon}{\partial y}\right) + \frac{\partial}{\partial z} \left(\frac{\nu_t}{\sigma_\varepsilon} \frac{\partial \varepsilon}{\partial y}\right)$$

$$+ c_1 \varepsilon \frac{P}{k} - c_2 \varepsilon^2/k \quad \ldots\ldots \quad (9)$$

where σ_k and σ_ε, c_1 and c_2 are empirical constants and P is the rate of energy production given by:

$$P = \nu_t \left(\left(\frac{\partial u}{\partial y}\right)^2 + \left(\frac{\partial u}{\partial z}\right)^2\right) \quad \ldots\ldots\ldots\ldots\ldots\ldots \quad (10)$$

The turbulent eddy viscosity is evaluated as

$$\nu_t = c_\mu k^2/\varepsilon \quad \ldots\ldots\ldots\ldots\ldots\ldots\ldots \quad (11)$$

where c_μ is an empirical constant.

The momentum equations (Eqs. 2-4) are simplified versions of the Reynold's equations. In deriving Equations 2-4, it is assumed that

the flow is predominantly in the x direction, and hence the x-gradient stress terms are neglected.

It is further assumed that the pressure term in the x-momentum equation is formed from a spatial-mean pressure over the yz plane to preserve the parabolic nature of the governing equation which is specially suited for marching-forward-type numerical schemes. The pressure gradient term in Eq. (2) is represented by the term $(-gdH/dx + g\sin\theta)$, which is the driving force for free surface flows. Furthermore, the turbulent shear stresses in the x-direction momentum equation are expressed in terms of an eddy viscosity ν_t in order to simplify the algebraic relations of turbulent shear stresses, i.e., equations 5, 6 and 7. However, the eddy viscosity representation is not used in the y or z momentum equations in order that the turbulence driven secondary circulation in the cross-section does not vanish (see Rodi (9)).

The values for the empirical constants in Equations (5), (6), (7), (9) and (11) are those given in Refs. 9 and 10 and no adjustments of constants were made. The values are: $c_1 = 1.43$, $c_2 = 1.92$, $c_\mu = 0.09$, $\sigma_k = 1.0$, $\sigma_\varepsilon = 1.3$, $c_{\phi_1} = 2.60$, $c_{\phi_2} = 0.365$, and $\beta = 0.0173$.

Boundary Conditions

The boundary conditions are to be specified at the solid boundaries and the free surface for the velocity components, u, v and w, the kinetic energy, k and the dissipation rate, ε.

The conditions of the solid boundaries are specified using the wall function technique proposed by Launder and Spalding (4). According to this technique, the conditions are specified at a grid point which lies outside the laminar sublayer. It is assumed that the shear stress and the velocity at this grid point satisfy the logarithmic portion of the universal law of the wall given by:

$$\frac{V}{V_*} = \frac{1}{\kappa} \ln\left(E \cdot \frac{V_* y_w}{\nu}\right) \quad \ldots\ldots\ldots\ldots\ldots\ldots \quad (12)$$

in which V is the resultant velocity along the boundary and V_* is the resultant friction velocity; y_w is the distance between the first grid point and solid boundary; κ is the von Karman constant and E is a parameter representing wall roughness. The value of E is evaluated using the following two expressions:

$$E = \exp \frac{(\kappa B_s)}{\left(\frac{V_* k_s}{\nu}\right)} \quad \ldots\ldots\ldots\ldots\ldots\ldots \quad (13)$$

and

$$B_s = \left[5.50 + 2.50 \ln \left(\frac{V_* k_s}{\nu}\right)\right] \exp\left\{-.217 \left[\ln \left(\frac{V_* k_s}{\nu}\right)\right]^2\right\}$$

$$+8.5 \left(1 - \exp\left\{- .217 \left[\ln\left(\frac{V_* k_s}{\nu}\right)\right]^2\right\}\right) \quad \ldots\ldots \quad (14)$$

in which k_s is the equilavent sand grain roughness of the solid boundary. The expression (14) for B_s is an approximation to Nikuradse's graph between B_s and log $(V_* k_s/\nu)$ over the entire turbulence regime ranging from hydraulically smooth turbulence to fully developed turbulence. This expression was first developed by Yalin (13) and has been applied by Krishnappan (2). Normal velocity components at the solid boundaries are set as zeros.

To specify conditions for k and ε at the grid point near the wall, it was assumed that the turbulence near the wall is in local equilibrium, i.e., the production rate is equal to the dissipation rate. Furthermore, it is assumed that the turbulent shear stress is equal to the wall shear stress. Under these assumptions, the expressions for k and ε at the wall region become:

$$k_w = \frac{V_*^2}{\sqrt{c_\mu}} \quad \ldots\ldots\ldots\ldots\ldots\ldots\ldots\ldots \quad (15)$$

$$\varepsilon_w = \frac{V_*^3}{\kappa\, y_w} \quad \ldots\ldots\ldots\ldots\ldots\ldots\ldots\ldots \quad (16)$$

The free surface boundary conditions for velocity and turbulent kinetic energy were specified following the approach of Rostogi & Rodi (8) which considers the free surface to act as a plane of symmetry. Therefore, the gradients of u, w, k in y direction and the vertical component v are zero. For specifying the condition for ε at the free surface, the approach of Lau & Krishnappan (3) was adopted. According to this approach, ε at the free surface was evaluated using the following relationship.

$$\varepsilon_f = \frac{c_f \left(\frac{k_f}{\sqrt{c_\mu}}\right)^{3/2}}{\kappa\, y_f} \quad \ldots\ldots\ldots\ldots\ldots\ldots\ldots\ldots \quad (17)$$

where k_f is the kinetic energy at the free surface and y_f is the distance between the nearest grid point and the surface and c_f is an empirical constant. The value of c_f used is 0.164, as given by Ref. 3.

Numerical Scheme

The form of equations (2), (3), (4), (7) and (8) is similar and hence all these equations can be expressed by a single equation of the following general form:

$$u \frac{\partial \phi}{\partial x} + v \frac{\partial \phi}{\partial y} + w \frac{\partial \phi}{\partial z} = \frac{\partial}{\partial y} (\Gamma_\phi \frac{\partial \phi}{\partial y}) + \frac{\partial}{\partial z} (\Gamma_\phi \frac{\partial \phi}{\partial z}) + s_\phi \quad \ldots \quad (18)$$

Equation (18) for example, transforms into Equation (2) when ϕ is equated to u; Γ_ϕ to $(\nu + \nu_t)$ and s_ϕ to $(-g\sin\theta + g\, \partial H/\partial x)$.

Since the governing equations are all expressible by a single equation of the form of Eq. (18), a single numerical algorithm can be used to solve all the equations. For the present work, the numerical scheme proposed by Patankar and Spalding (7) was employed. Patankar and Spalding used a finite difference approach to solve the equations, in which the difference equations were derived by integrating the governing equations term by term over small control volumes.

The grid system used in the present study is shown in Fig. 2. Referring to Fig. 2, by assigning different values to IBL, IBR, JB, NP3 and MP3, it is possible to define compound channel cross-sections with different ratios of channel width to flood plain width and channel depth to flood plain depth. This grid system can also treat symmetric as well as asymmetric flood plains and can be used for a single rectangular or square cross section channels. The roughness of each boundary element is specified independently and hence it is possible to investigate the effect of different roughnesses.

MODEL APPLICATION

The model was applied to simulate some of the experimental runs of Myers and Elsawy (5), Wormleaton et al. (11) and Knight and Demetriou (1) so that the model predictions can be compared with the experimental data reported. The channels used in the three investigations are illustrated in Fig. 3. Myers and Elsawy (5) used an asymmetric compound channel whereas the other investigators used symmetric channel sections.

In running the model, the channel slope, flow depth and boundary roughnesses were specified. The discharge, velocity distribution and shear stress distribution were then obtained from the model predictions. The model started with certain arbitrary assumptions for u, v, w, k and ε at the upstream boundary and calculated the flow conditions at a section located at a distance of Δx downstream. Using the calculated flow conditions as initial conditions for the next section, the model calculations proceeded in the downstream direction until uniform flow conditions are achieved. Uniform flow conditions were tested by computing the frictional slope S_f as

$$S_f = \frac{\int \tau_0 dP}{A\gamma} \qquad \ldots\ldots\ldots\ldots\ldots\ldots\ldots\ldots \quad (19)$$

in which τ_0 is the boundary shear stream, dP is a small segment of the wetted parimeter, A is the cross-sectional area of flow and γ is the specific weight of fluid.

When channel slope and S_f were approximately equal, the variation in flow conditions along the channel were negligible and uniform flow conditions were established. The flowrate was then computed as the integral of the longitudinal velocity component over the cross-sectional area. It was observed that the computed uniform flow conditions did not depend on the initial distribution assumed for u, v, w, k and ε at the upstream boundary and hence uniform distributions for u, k and ε and zero values for v and w were assumed initially in all of the model simulations presented here.

For some of the runs, the values of the flow depth H specified to the model were not exactly equal to the values of H in the experimental runs. The reason is that the selection of the size of grid spacing was made with the constraint that the bottom of the main channel, the bottom of the flood plain and the free surface must all

coincide with horizontal grid lines. Because the size of the channel was fixed, the vertical grid size must be some fraction of the distance from the bottom of the flood plain to the bottom of the main channel. Using this chosen grid size, the actual water surface in the experimental runs would not necessarily coincide with a grid line. To make the water surface coincide with a grid line would usually make the grid sizes too small and would require a large storage capacity to run the model. Therefore, when necessary, it was decided to simulate runs in which the total depth was very close but not exactly equal to the actual depth in the experiments. For example in the simulation of run #1 of Myers & Elsawy (5) a grid spacing of 1.693 cm was selected for both horizontal and vertical grid lines. This resulted in a total grid spacing of 36 in the horizontal direction and 10 in the vertical direction and IBR and JB (Fig. 2) assumed values of 17 and 8 respectively. The total flow depth H of the simulated flow became 16.93 cm which is very close to the actual depth of 16.89 cm.

Flows with very shallow flood plain depths also require fine grid spacings resulting in storage capacity requirements that exceed the available capacity of the CDC Cyber 371 computer used in this study. Simulations were therefore not carried out for those runs.

The longitudinal grid size was set at 1/50 of the total flow depth for all the simulations.

COMPARISON WITH EXPERIMETAL DATA

Data of Myers and Elsawy (5)

Myers and Elsawy tested ten flows in their asymmetric channel (Fig. 3) made of smooth perspex. The channel slope was maintained at a constant value of 0.00026. The flow rates, flow depths and shear stress distributions were reported.

Runs #1, #4, and #7 from Ref. 5 were chosen for the model simulation. The hydraulic data from these runs are summarized in Table 1 together with the predictions of the model. It can be seen

from Table 1 that the agreement between the predicted and measured flow rates is very reasonable. The measured shear stress distributions around the wetted perimeter are compared with the predicted distributions in Fig. 4 for the three runs. It can be seen that the model predictions of shear stress distributions are also in reasonable agreement with the measured data.

Data of Knight and Demetriou (1)

Knight and Demetriou conducted their experiments in a symmetric channel of smooth perspex, in which the flood plain widths could be altered by adjustable sidewalls. The slope of the channel was kept constant. Velocity and shear stress distributions were measured. From the velocity distributions the percentage of flow carried by the main channel and flood plains were computed and reported. From the measured shear stress distributions, the percentage of the total shear force acting on the different sections of the wetted perimeter was calculated and reported.

All the boundaries in the channel used by Knight and Demetriou were made to coincide with the numerical grid lines. However, the flow depths of the simulated runs were slightly different from the experimental values. Simulations were carried out for twelve of the twenty-four experimental runs reported. The results are summarized in Table 2.

It can be seen from Table 2 that the values of discharge computed compare fairly well with those measured. The percentage of the total flow moving through the main channel section with imaginary vertical walls was computed and is plotted in Fig. 5 as functions of (H-h)/H, with B/b as parameter. The agreement with the data of Knight and Demetriou is quite good.

From the shear stress distributions predicted by the model, the percentage shear force acting on different segments were computed and are compared with the experimental data in Fig. 6. The

experimental data of Knight et al covered a range of 2 to 5 for the parameter B/b and .106 to .505 for the parameter (H-h)/H. For the simulated runs, the range of B/b is the same but the range for (H-h)/H is only between .286 and .50. The lower values of (H-h)/H required finer numerical grid and hence large computer memory which exceeded the limit of the computer used in the present study. Nevertheless, it is possible to make a comparison of the model results with the results of Ref. 1 as shown in Figs. 5 and 6. The solid lines in Figs. 5 and 6 are drawn through the data of Knight and Demetriou whereas the points represent the results of the numerical model. It can be seen that the trends predicted by the model are in reasonable agreement with the experimental data.

Data of Wormleaton et al (11)

The experiments were conducted in a symmetric channel in which the main channel was made of perspex while the flood plains were made of concrete with various roughnesses. Forty tests were conducted using different combinations of flow depths, channel slopes and boundary roughnesses.

Eight out of the forty runs were simulated using the model. A vertical grid size of 2.0 cm permitted the exact flow depths to be simulated. However, the horizontal grid size could not be made such that all the vertical sides of the flood plain and main channel coincide with a grid line. Therefore the width of the main channel used in the model was 28.23 cm instead of the 29.0 cm in the experiments.

Wormleaton et al (11) gave the boundary roughnesses in terms of Manning's n. To express this in terms of the equivalent sand grain roughness, k_s, used in the model, the following Strickler relationship was used

$$n = \frac{k_s^{1/6}}{51.79} \qquad (k_s \text{ in cm}) \tag{20}$$

The experimental data and the model predictions are summarized in Table 3. The predicted and measured flow rates are compared in Fig. 7. The flowrates predicted by the model are slightly on the higher side for a few of the runs. However, the maximum deviation is only 7%. Therefore the agreement between the predicted and measured flow rates for the flows tested by Wormleaton et al can be considered as reasonable.

The division of flow between the main channel and flood plain was calculated by Wormleaton and Hadjipanos (12) using point velocity measurements over the flow cross section. These results showed that the various methods of discharge calculation using Manning's formula cannot predict the division of flow with any degree of accuracy, even when the overall discharge was predicted satisfactorily. Their data for the cases of smooth (series A) and roughened (series C) flood plains, with vertical interface planes, are plotted in Fig. 8. Simulations were also carried out using 6 cm and 8 cm floodplain depths and the division of flow was obtained from the predicted velocity distributions. The results, plotted in Fig. 8, show reasonable agreement with the measurement. The model overestimated the main channel discharge somewhat but the errors are all less than five percent and can be considered to be very satisfactory, especially when compared with errors of up to sixty percent as given in Ref. 12.

SUMMARY AND CONCLUSIONS

The turbulence model described in this paper has been applied to calculate the flow characteristics in different compound channels. Using specified boundary roughnesses, channel slope and flow depth, the model predicts the total flow rate, shear stress distribution around the wetted perimeter and the velocity distribution, from which the division of flow and shear force between the main channel and flood plain can be computed.

Comparisons with the published data show that the discharge in different compound channels can be predicted quite well with the model. Comparisons with the data of Myers and Elsawy (5) show that the shear stress distributions can also be predicted reasonably well. Using the data of Knight and Demetriou (1) and Wormealton et al (11) the model has been shown to be capable of predicting the division of shear force around the wetted perimeter and the division of flow carried by the flood plain and main channel sections. More data on shear stress distributions, as well as data on velocity distributions, would enable one to validate the model for wider ranges of flow conditions. However, it appears that the present model should be a very useful tool for investigating the characteristics of flows with flood plains.

ACKNOWLEDGEMENTS

The authors wish to acknowledge the assistance of Dr. W.R.C. Myers and Dr. P.R. Wormleaton in providing their data on stress measurements and flow rates.

TABLE 1. Comparison of Model Predictions with Data of Myers and Elsawy (5)

Run No.	Flowdepth H in cm		Slope S		Flowrate Q l/s in litres per second	
	Actual	Used in Model	Slope of Channel	Predicted in Model S_f	Actual	Predicted by Model
1	16.89	16.93	.00026	.000261	18.41	18.49
4	15.33	15.24	.00026	.000253	14.16	13.96
7	13.34	13.54	.0026	.000250	9.91	11.20

TABLE 2. Comparison of Model Predictions with Data of Knight and Demetriou (1)

Actual or Simulated Run	$\frac{B}{b}$	H, in millimetres	Q, in litres per second	τ_o, in newton per squared metre	Shear Force, SF, in newton per metre	$\frac{(H-h)}{H}$	Shear Forces in % of SF				Flowrates in % Q	
							2(i)	2(ii)	2(iii)	(iv)	main channel	flood plain
Actual	2	149.8	17.1	0.533	0.322	0.493	21.7	26.9	26.5	24.9	69.3	30.7
Simulated	2	152.0	17.8	0.544	0.331	0.500	4.3	24.7	25.9	25.1	70.7	29.3
Simulated	2	136.8	14.7	0.484	0.294	0.444	19.6	25.5	27.8	27.1	73.3	26.7
Actual	2	125.8	11.7	0.455	0.253	0.396	13.8	27.5	29.8	28.9	75.1	24.9
Simulated	2	121.6	11.5	0.440	0.241	0.375	12.3	24.6	31.5	31.7	78.4	21.6
Actual	2	100.3	7.3	0.356	0.179	0.242	5.2	24.4	34.4	36.0	86.3	13.7
Simulated	2	106.4	7.3	0.285	0.148	0.286	6.3	20.	35.5	37.6	85.0	15.0
Actual	3	149.2	23 4	0.564	0.426	0.491	16.3	44.0	20.1	19.6	52.4	47.6
Simulated	3	152.0	24.5	0.577	0.439	0.500	17.0	40.9	21.4	20.7	53.4	46.6
Simulated	3	136.8	19.5	0.518	0.378	0.444	12.8	41.8	23.0	22.5	57.1	42.9
Actual	3	125.0	15.2	0.455	0.321	0.392	10.3	44.2	22.8	22.7	60.2	39.8
Simulated	3	121.6	14.8	0.448	0.313	0.375	7.7	39/7	26.1	26.5	63.9	36.1
Actual	3	100.9	8.1	0.33	0.217	0.247	5.0	42.0	26.2	26.8	74.1	25.9
Simulated	3	106.4	10.6	0.378	0.253	0.286	7.4	45.7	22.2	24.6	68.7	31.3
Actual	4	153.8	29.4	0.609	0.559	0.506	12.7	53.9	16.9	16.5	40.3	59.7
Simulated	4	152.0	31.6	0.616	0.562	0.500	13.7	50.7	18.1	17.5	42.9	57.1
Simulated	4	136.8	24.4	0.536	0.473	0.444	10.2	51.7	19.3	18.9	46.7	53.3
Actual	4	127.4	18.0	0.470	0.406	0.403	8.7	54.6	18.7	18.0	47.7	52.3
Simulated	4	121.6	18.2	0.473	0.403	0.375	6.3	51.3	21.2	21.3	52.9	47.1
Actual	4	102.1	9.1	0.320	0.260	0.256	6.7	52.3	21.1	23.0	63.2	36.8
Simulated	4	106.4	10.3	0.287	0.235	0.286	5.8	56.2	18.9	19.1	58.2	41.8

TABLE 3. Comparison of Model Predictions with the Data of Wormleaton et al. (11)

Run No.	Total Depth, H, in cm		Channel Slope S		Boundary Roughness		Flowrate, Q, in litres per second	
	Actual	Model	Actual	Actual Model S_f	Manning 'n'	Equiv. Sand Roughness, in cm	Actual	Predicted by Model
A6	18	18	.00043	.000425	smooth	0	37.0	38.71
B4	18	18	.00043	.000426	.014	.145	31.0	32.47
C5	18	18	.00043	.000426	.017	.466	28.0	29.77
C7	20	20	.00043	.000428	.017	.466	37.0	39.8
D5	18	18	.00043	.000434	.021	1.654	240	25.33
D7	20	20	.00043	.000432	.021	1.654	33.0	33.26
D11	18	18	.00094	.00072	.021	1.654	35.5	36.4
D14	18	18	.00132	.00127	.021	1.654	42.0	42.12

FIGURE CAPTIONS

Figure 1. Definition sketch.

Figure 2. Grid system.

Figure 3. Experimental channels of Refs. 1, 5 and 11.

Figure 4. Comparisons of predicted and measured shear stress distributions - data of Myers and Elsawy (5).

Figure 5. Comparisons of predicted and measured percentages of total flow carried by main channel - data of Knight and Demetriou (1).

Figure 6. Comparison of predicted and measured % shear force on various boundaries - data of Knight and Demetriou (1).

Figure 7. Comparisons of predicted and measured flow rates - data of Wormleaton et al. (11).

Figure 8. Comparisons of predicted and measured percentages of total flow carried by main channel - data of Wormleaton et al. (11).

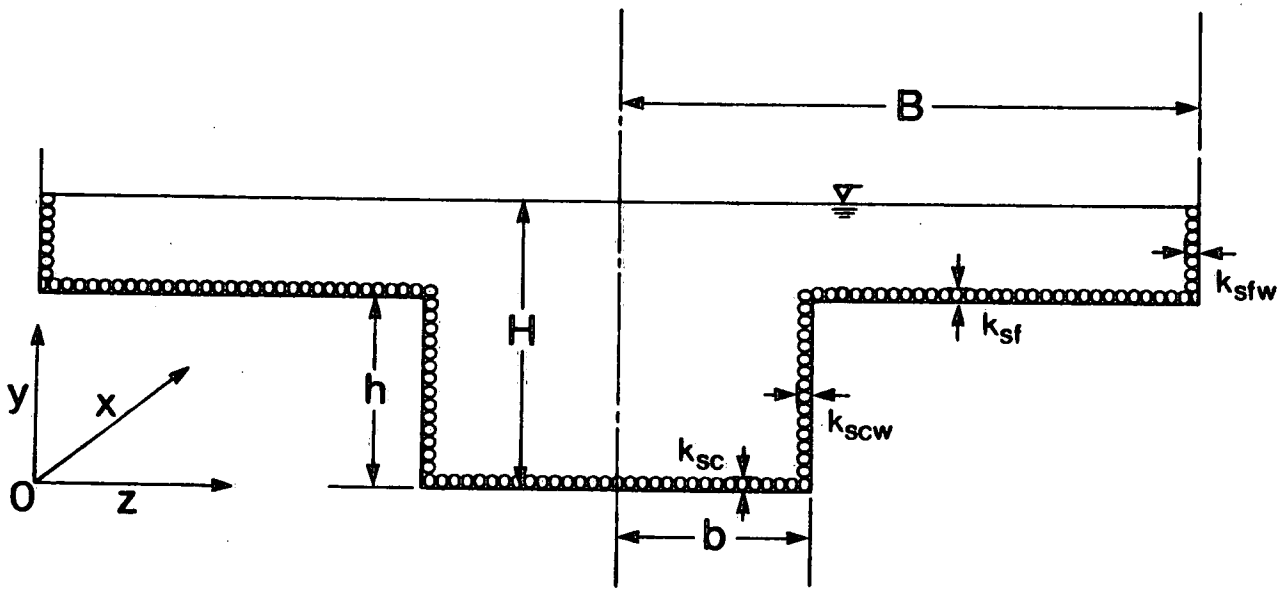
B
H
h
y
x
0
z
k_{sfw}
k_{sf}
k_{scw}
k_{sc}
b

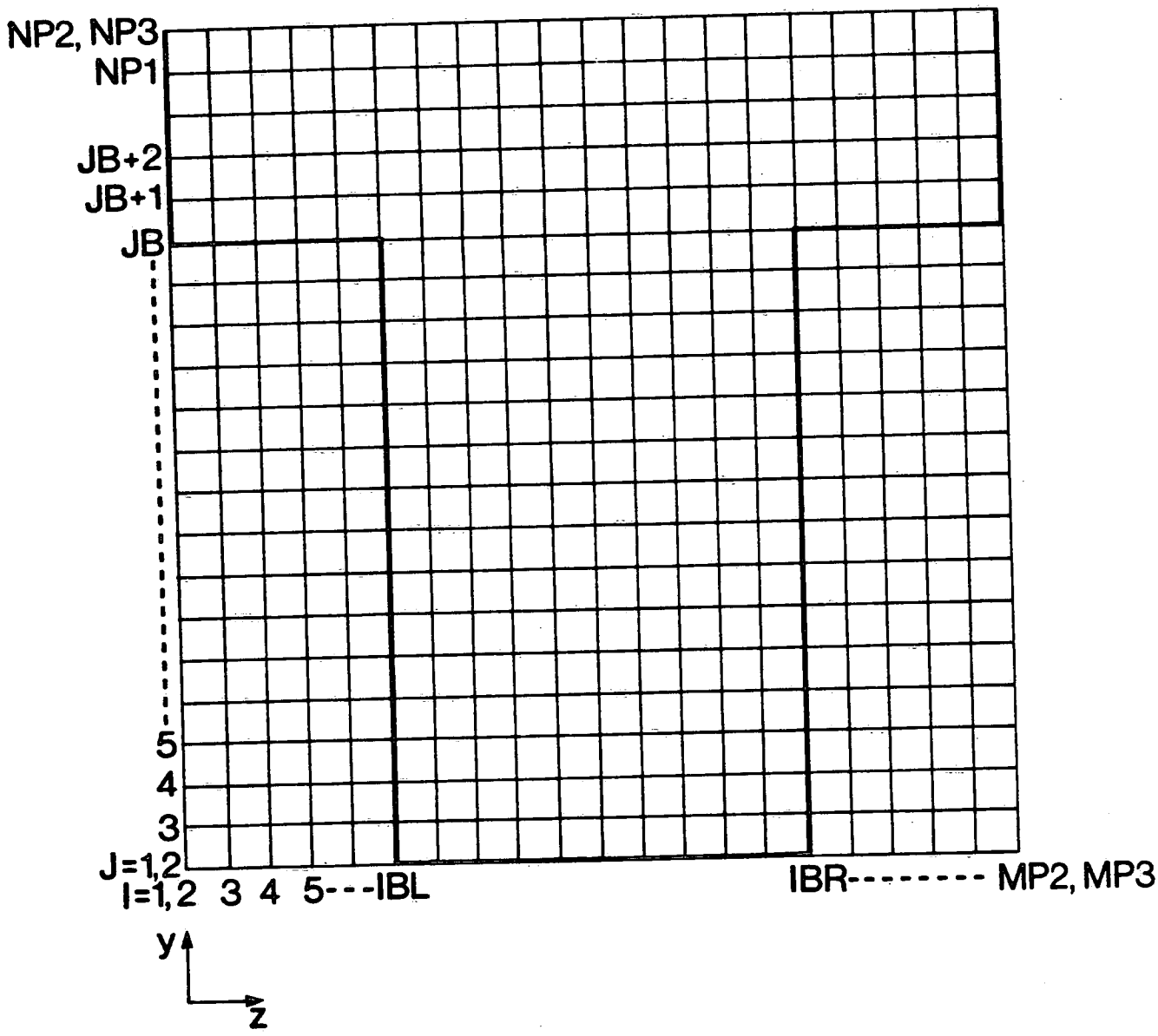

Fig 2

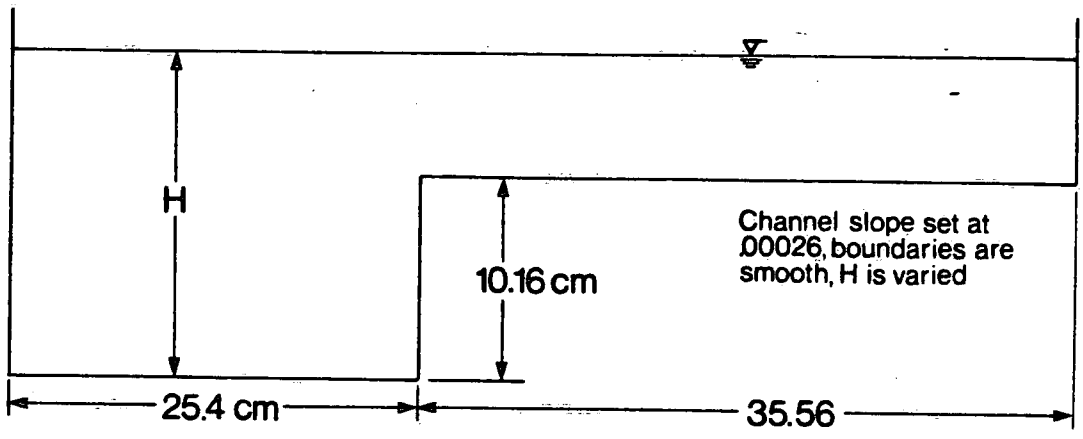

(a) MYERS and ELSAWY

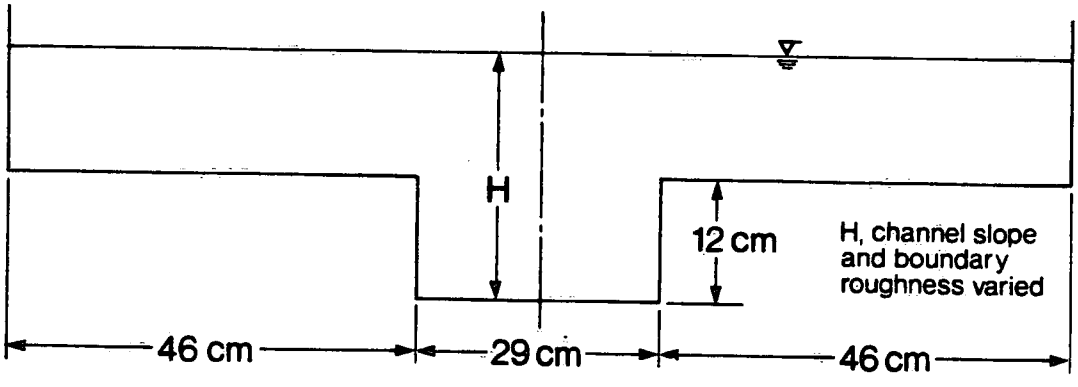

(b) WORMLEATON et al

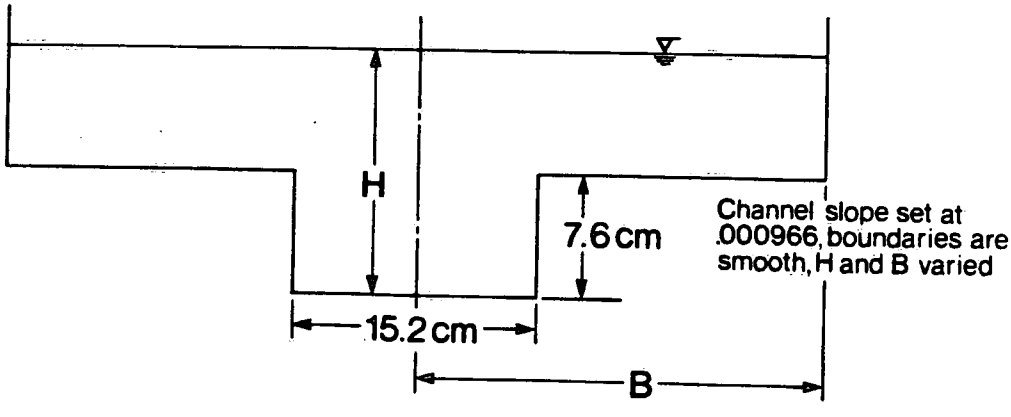

(c) KNIGHT et al

Fig 3

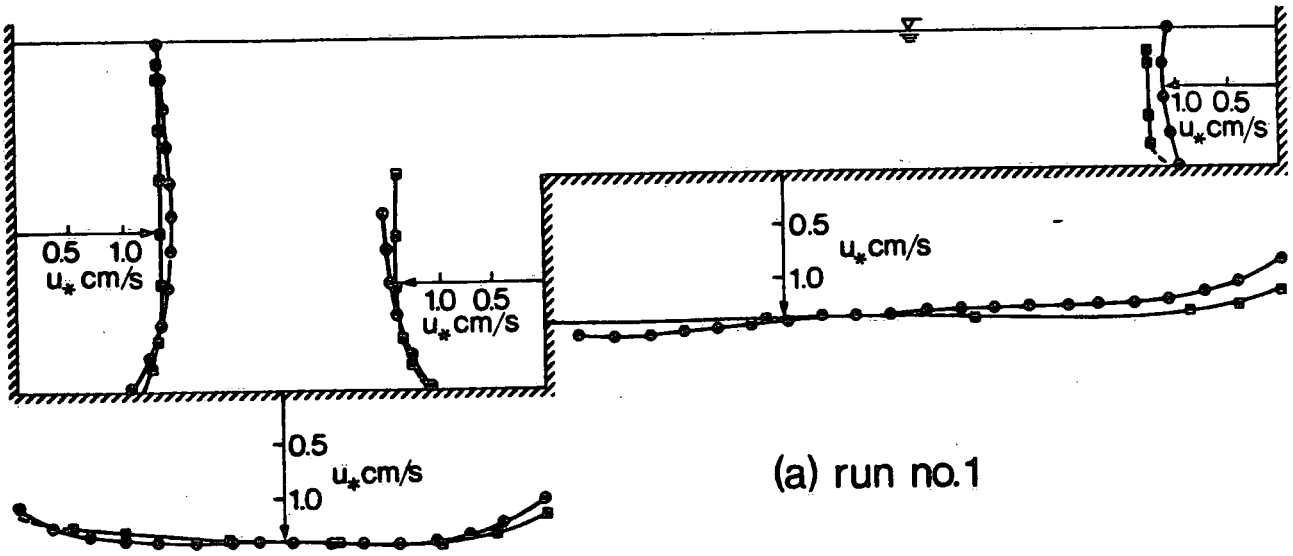

(a) run no.1

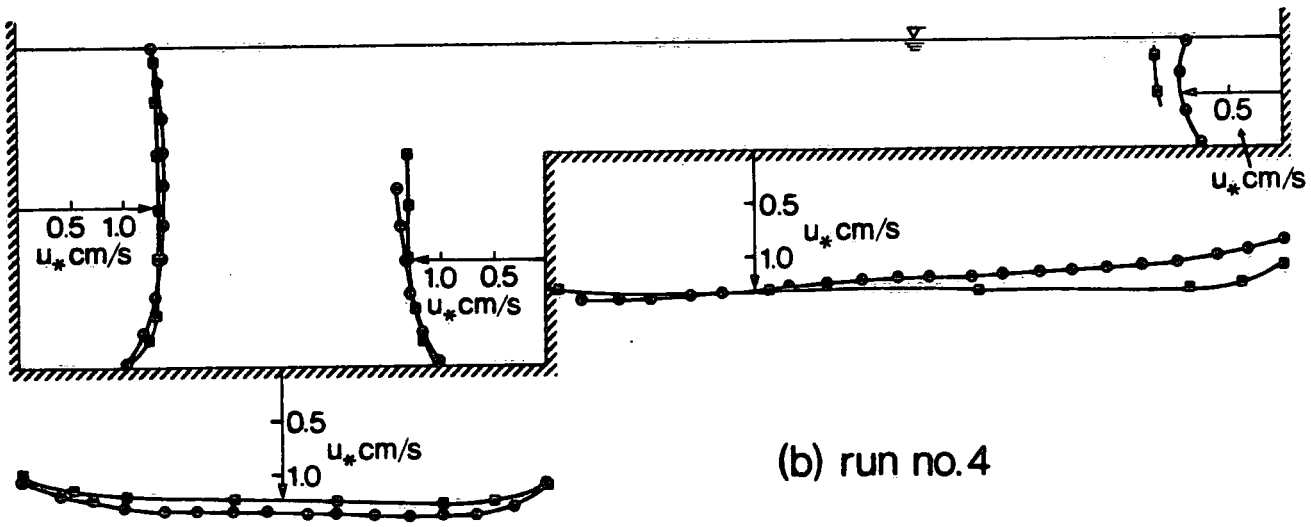

(b) run no.4

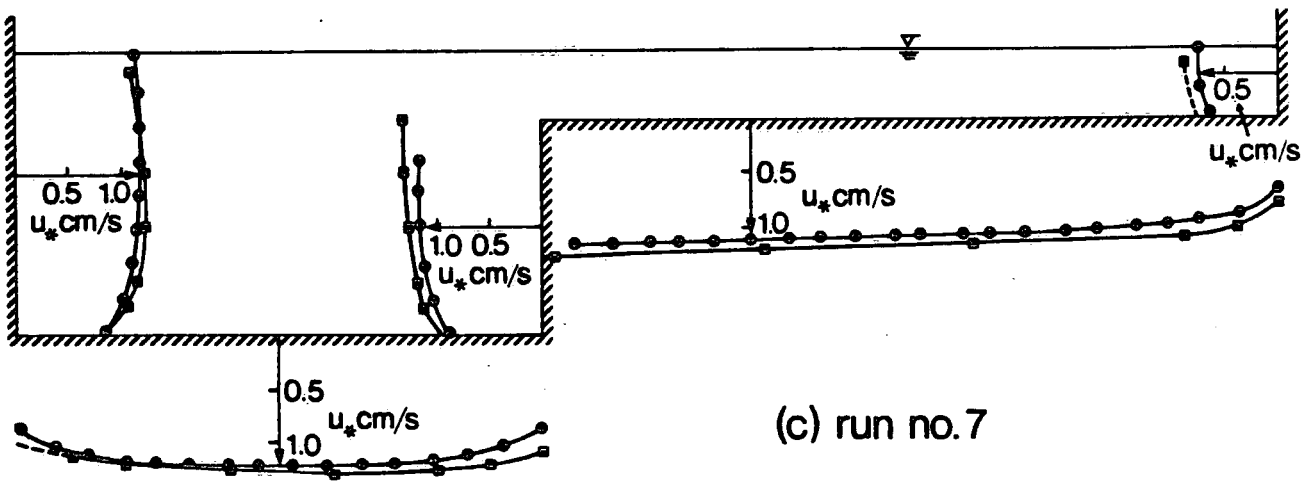

(c) run no.7

measurement

model predictions

Fig.4

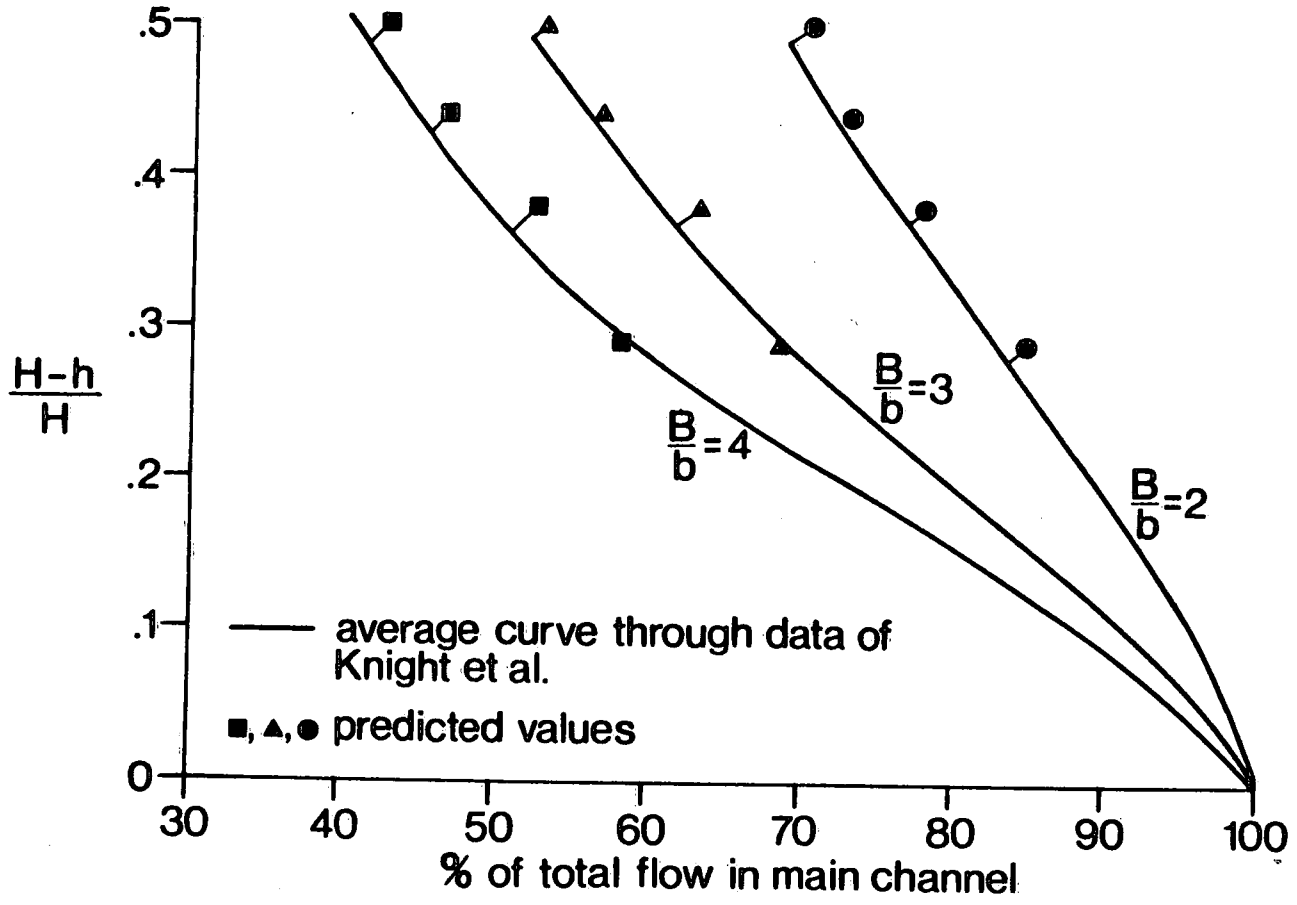
.5
.4
.3
.2
.1
0
H-h / H
B/b=4
B/b=3
B/b=2
average curve through data of Knight et al.
■, ▲, ● predicted values
30
40
50
60
70
80
90
100
% of total flow in main channel

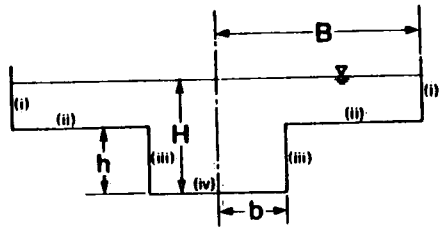

——— smooth line drawn through experimental data of Knight et al

■,●,▲,□ values predicted by model

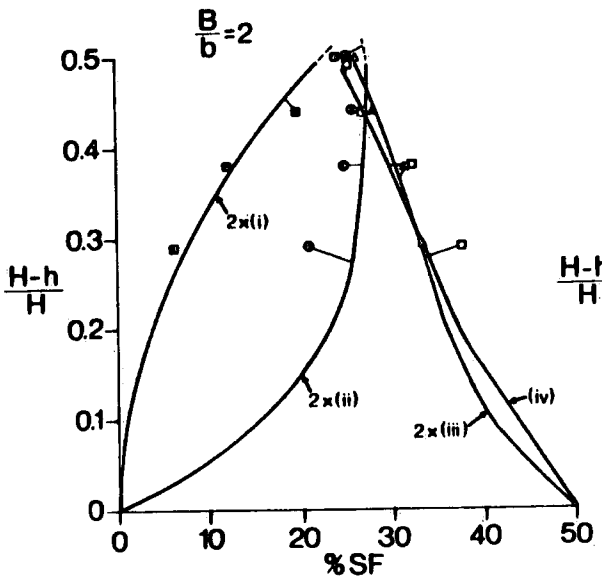

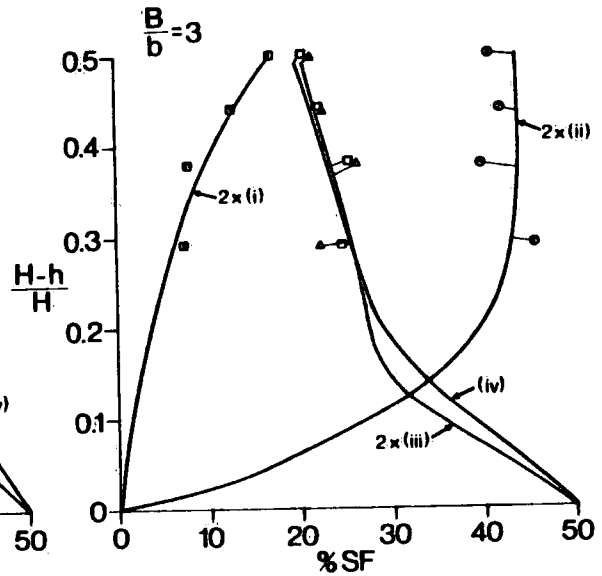

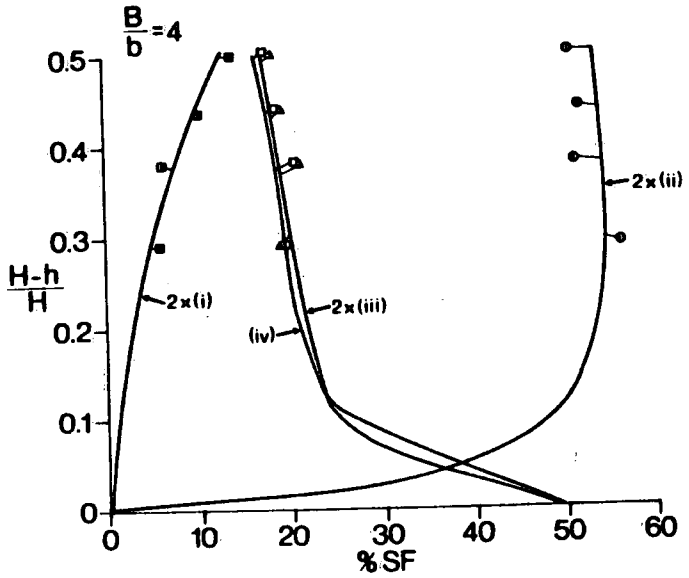

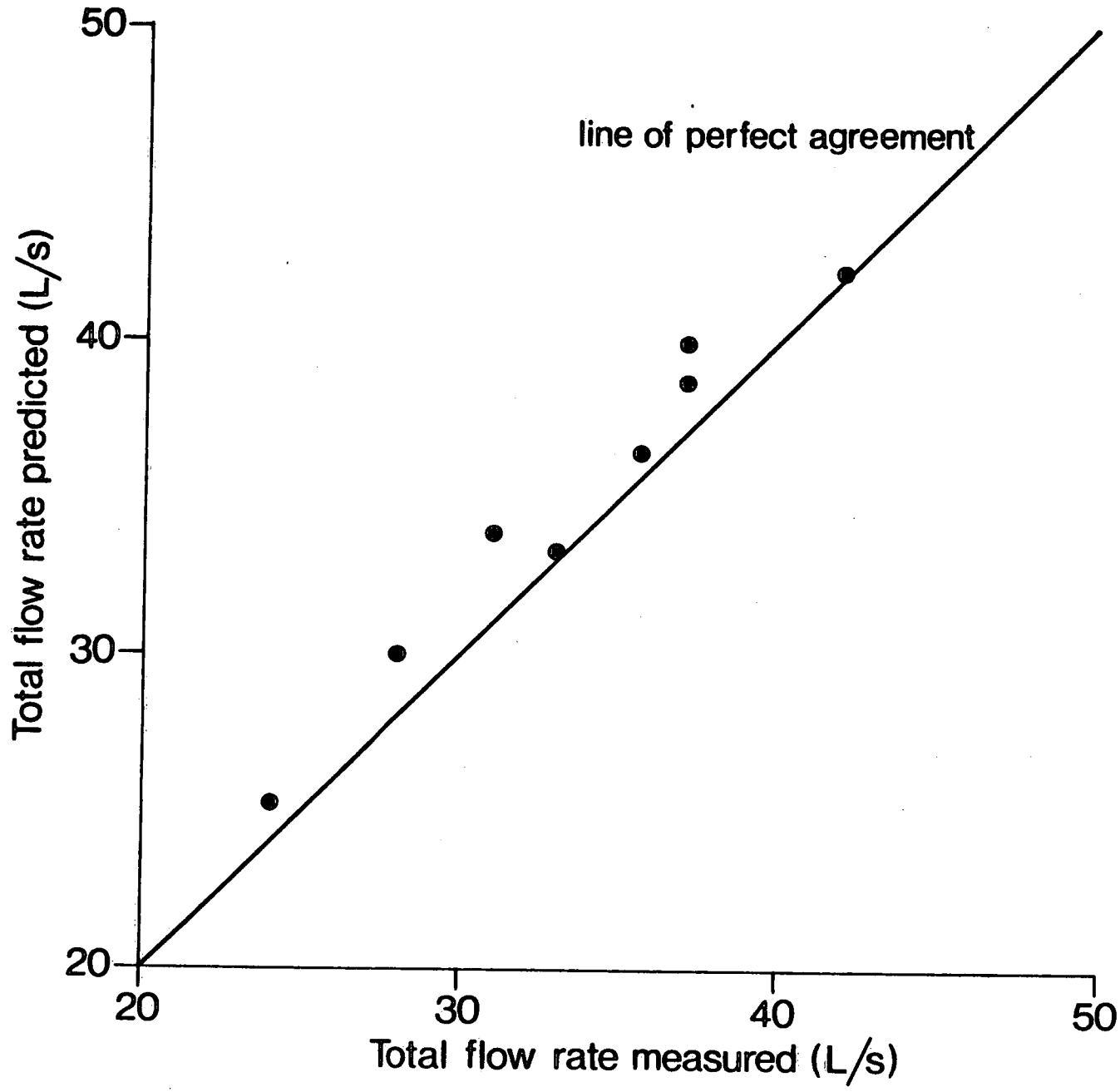
50
40
30
20
Total flow rate predicted (L/s)
line of perfect agreement
20
30
40
50
Total flow rate measured (L/s)

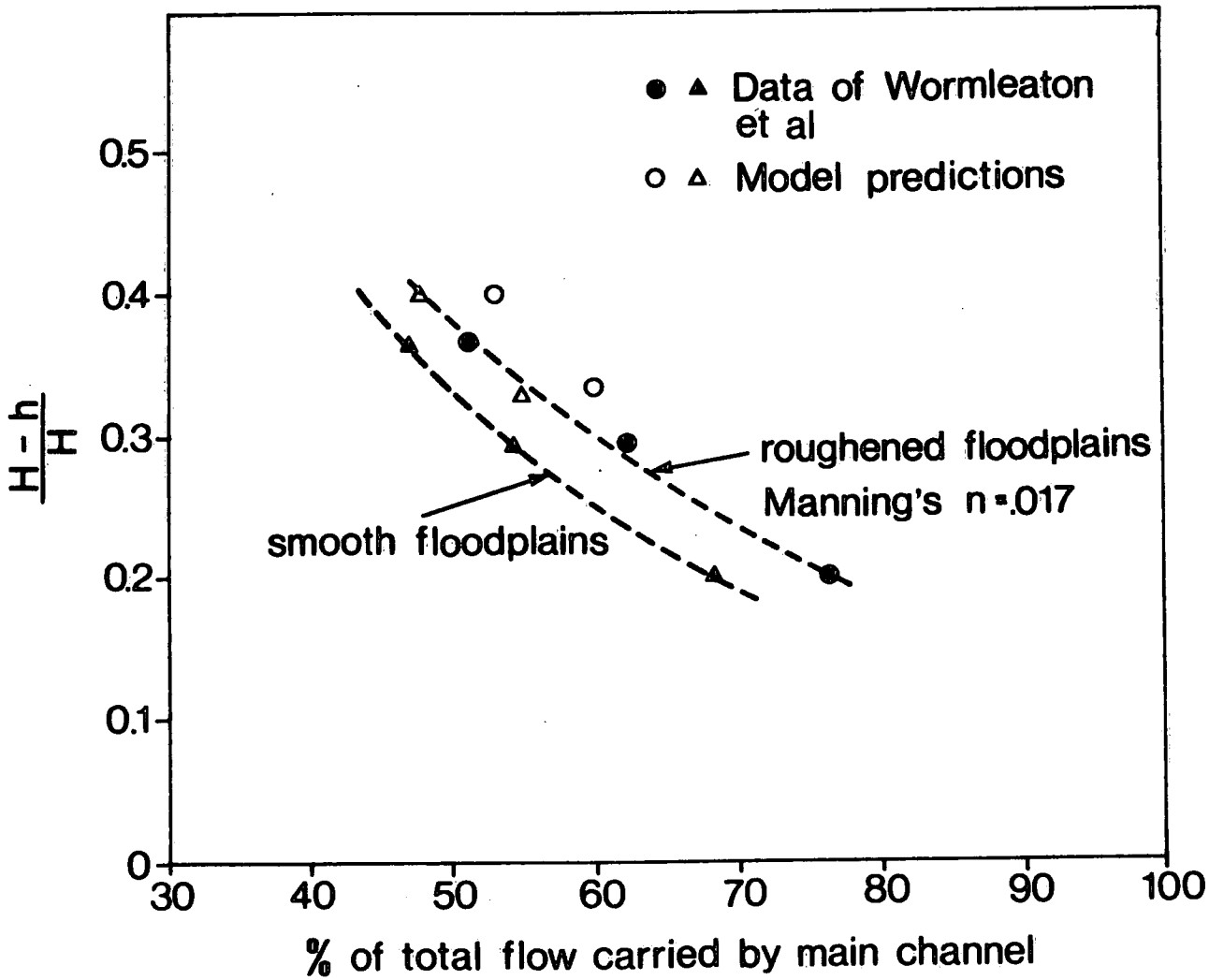
● ▲ Data of Wormleaton et al
○ △ Model predictions
roughened floodplains
Manning's n=.017
smooth floodplains
0.5
0.4
0.3
0.2
0.1
0
H-h/H
30
40
50
60
70
80
90
100
% of total flow carried by main channel

APPENDIX 1 - REFERENCES

1. Knight, D.W., and Demetriou, J.D., "Flood Plain and Main-Channel Flow Interaction," Journal of Hydraulic Engineering, 109, No. 8, August 1983, pp. 1073-1092.
2. Krishnappan, B.G., "Laboratory Verification of Turbulent Flow Model," Journal of Hydraulic Engineering, 110, No. 4, April 1984, pp. 500-514.
3. Lau, Y.L. and Krishnappan, B.G, "Ice Cover Effects on Stream Flows and Mixing," Journal of the Hydraulics Division, Proc. ASCE, 107, No. HY10, Oct. 1981, pp. 1225-1242.
4. Launder, B.E. and Spalding, D.B., "The Numerical Computation of Turbulent Flow," Computer Methods in Applied Mechanics and Engineering, 3, 1974, pp. 269-289.
5. Myers, W.R.C. and Elsawy, E.M., "Boundary Shear in Channel with Flood Plain, "Journal of the Hydraulics Divison, ASCE, 101, No. HY7, July 1975, pp. 933-946.
6. Noat, D. and Rodi, W., "Calculation of Secondary Currents in Channel Flow, "Journal of the Hydraulics Division, Proc. ASCE, 108, No. HY8, Aug. 1982, pp. 948-968.
7. Patankar, S.V. and Spalding, D.B., "A Calculation Procedure for Heat, Mass and Momentum Transfer in Three-Dimensional Parabolic Flows, "Int. Journal of Heat and Mass Transfer, 15, pp. 1787 to 1806, 1972, Pergamon Press, G. Britain.
8. Rastogi, A.K. and Rodi, W.," Predictions of Heat and Mass Transfer in Open Channels," Journal of the Hydraulics Divison, Proc. ASCE 104, No. HY3, March 1978, pp. 397-419.
9. Rodi, W., "Turbulence Models and Their Applications in Hydraulics," State-of-the-art Paper, presented by the IAHR-Section on Funadmentals, Division II: Experimental and Mathematical Fluid Mechanics, June 1980.
10. Tatchell, D.G., "Convection Processes in Confined Three-Dimensional Boundary Layers," thesis presented to Imperial College of London, England, in 1975, in fulfillment of the requirements for the degree of Doctor of Philosophy.

11. Wormleator, P.R., Allen, J., and Hadjipanos, P., "Discharge Assessment in Compound Channel Flow, "Journal of the Hydraulics Division, Proc. ASCE, 108, No. HY9, Sept. 1982, pp. 975-994.

12. Wormleaton, P.R. and Hadjpanos, P., "Flow Distribution in Compound Channels," Journal of Hydrualic Engineering, ASCE, Vol. 111, No. 2, February 1985, pp. 357-361.

13. Yalin, M.S., Private Communication.

APPENDIX II - NOTATION

The following symbols are used in this paper:

A = cross-sectional area of the flow;
B = half width of the total cross-section;
E = wall roughness parameter;
H = total depth of flow;
P = rate of production of turbulent energy;
Q = total discharge;
S = slope of channel;
S_f = frictional slope;
V = resultant velocity;
$V*$ = wall shear velocity;
b = half width of main channel;
c_1, c_2, c_μ, $c_{\phi 1}$, $c_{\phi 2}$, c_f = empirical constants;
g = gravitational acceleration;
h = distance between flood plain bottom and main channel bottom;
k = turbulent kinetic energy;
k_s = equivalent sand grain roughness;
k_w = value of turbulent kinetic energy at near wall grid point;
k_f = value of turbulent kinetic energy at free surface;
n = Manning's roughness;
p = pressure;
u = time averaged velocity in x direction;
v = time averaged velocity in y direction;
w = time averaged velocity in z direction;

x = longitudinal coordinate;
y = vertical coordinate;
z = lateral coordinate;

β = empirical constant;
θ = angle of inclination of channel;
ϵ = energy dissipation rate;
κ = von-Karman constant;
γ = specific weight of fluid;
ν = turbulent eddy viscosity;
ν_t = turbulent eddy viscosity;
σ_K, σ_E = empirical constants; and

τ_o = boundary shear stress;